A realistic kinetic Monte Carlo simulation of the faceting of a Pt(110) surface under reaction conditions

M. I. Monine and L. M. Pismen
Department of Chemical Engineering, Minerva Center for Nonlinear Physics of Complex Systems and Institute of Catalysis Science and Technology, Technion, 32000 Technion City, Haifa, Israel

R. Imbihl
Institut für Physikalische Chemie und Elektrochemie, Universität Hannover, Callinstrasse 3-3a, D-30167 Hannover, Germany

(Received 13 February 2004; accepted 30 August 2004)

The faceting process on Pt(110) is studied with the help of a kinetic Monte Carlo model taking into account realistic Pt–Pt, Pt–CO, and Pt–O interactions. The activation energies of the allowed atomic steps are estimated using available computational and experimental data. The model well reproduces the region in the parameter space where faceting occurs. Under kinetic instability conditions, the simulated faceted pattern forms a periodic hill and valley structure with a lateral periodicity of ~140–170 Å, which is comparable with experimental data. The simulations reproduce the development of faceting on a realistic time scale. © *2004 American Institute of Physics.* [DOI: 10.1063/1.1808417]

I. INTRODUCTION

Morphological changes of metal catalysts under operation conditions are common phenomenon in industrial catalysis. Well-known examples are the roughening of Pt/Rh gauzes in catalytic ammonia oxidation, the faceting of Ag catalysts in methanol oxidation, and also catalytic carbon monoxide oxidation on noble metal catalysts show pronounced effects (~1 atm).[1–3] In general, very little is known about the mechanism of these reaction-induced substrate changes under high pressure conditions but single crystal studies of CO oxidation on Pt revealed that reaction-induced substrate changes are also occurring under low pressure conditions.[4–10] These studies provided a rather detailed picture of how the substrate changes on a Pt(110) surface are linked to a kinetic instability of the reaction. Here we attempt to conduct a realistic three-dimensional (3D) modeling of the reaction-induced roughening/faceting of Pt(110) incorporating details of the adsorption process as well as an atomistic picture of the surface phase transition (SPT) $1\times2\rightleftharpoons1\times1$ of Pt(110).

The clean Pt(110) surface exhibits a 1×2 ''missing row'' reconstruction which is lifted upon adsorption of CO forcing the surface Pt atoms back into the bulklike 1×1 termination.[11–13] The origin of faceting was shown to be linked to kinetic instabilities, e.g., kinetic oscillations. These are caused by the surface phase transition which modulates the catalytic activity of the surface. It was found that the Pt(110) surface undergoes faceting during catalytic CO oxidation if reaction conditions are adjusted such that the CO induced $1\times2\rightleftharpoons1\times1$ SPT accompanies the reaction.[4–10] The mass transport of 50% of the surface atoms that is associated with the transition between the 1×1 and 1×2 missing row reconstruction causes a surface roughening which may develop into faceting under appropriate conditions. The oscillations and the faceting occur in a temperature range $T\sim400-530$ K and pressure range $p\sim10^{-5}-10^{-4}$ mbar.

Changes in the catalyst morphology are often associated with the activation or deactivation process. This is a common phenomenon in heterogeneous catalysis[1–3] which is also observed with CO oxidation on Pt(110). Instead of oscillatory changes obtained on a flat surface, a Pt(110) surface undergoing faceting shows a continuous rise of the CO_2 production rate. The increase of the CO_2 production rate can be attributed to higher oxygen sticking coefficients on (100) steps forming the (430), (320), and (210) facets of hill-structure slopes. These orientations which all belong to the [001] zone can all be built up by (100) step and (110) terrace units. By increasing the density of (100) steps the inclination angle of the facets grows continuously until the limiting case of Pt(210) is reached where (100) step and (110) terrace units alternate. This surface exhibiting the highest density of steps also displays the highest catalytic activity.

Earlier high-resolution low-energy electron diffraction (LEED) experiments[8] demonstrated that the facets on Pt(110) have a symmetric sawtooth shape forming a regular structure with a lateral periodicity of ~200 Å in the $[1\bar{1}0]$ direction. Real space images of a Pt(210) surface which has undergone faceting during catalytic CO oxidation have been recorded using scanning tunneling microscopy (STM).[14] In contrast to Pt(110), the faceting of Pt(210) is associated with a decrease of the CO_2 production rate because the (100) step density is lowered by faceting.

Recent experimental studies of roughening and faceting in the $CO+O_2/Pt(110)$ system have been performed by Han Wei *et al.*[15] Here we shall reiterate briefly only the main experimental observations to be compared with our simulations. Faceting is observed only under specific reaction conditions illustrated with the help of Fig. 1(a).[9] The diagram shows the reaction rate r_{CO_2} versus p_{CO} with p_{O_2} and T being

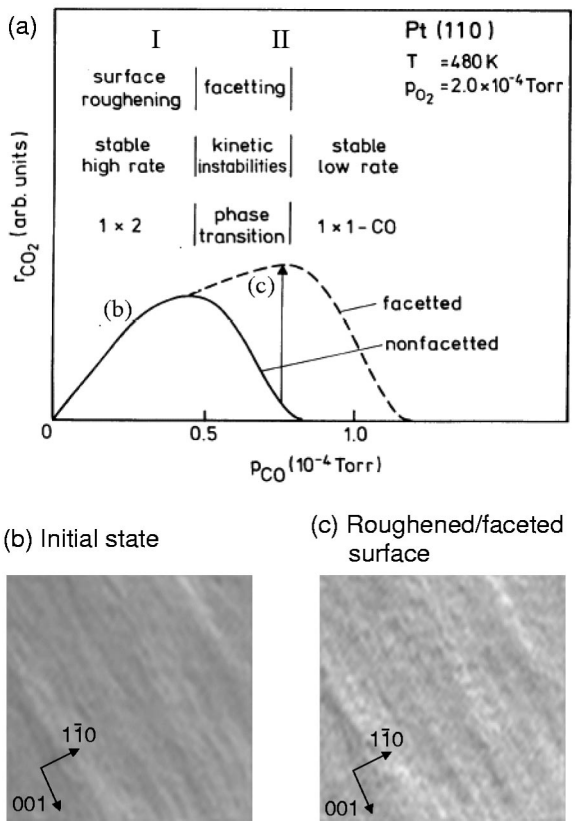

FIG. 1. Reaction-induced roughening/faceting in experiment. (a) Experimental conditions for different regimes of catalytic CO oxidation on Pt(110) (Ref. 9). The different regions indicated on top of the rate curve refer to an unfaceted Pt(110) surface. (b,c) LEEM images showing surface topographical changes due to reaction-induced roughening. Field of view is 2.4 μm, $T=427$ K, p_{CO} in the 10^{-5} mbar range. Initial surface (shortly after start of reaction) is shown in (b). Strongly roughened/faceted surface after exposure to the reaction for $\approx$30 min is shown in (c). The same area as in (b) is displayed. Note that the visual impression of a hill and valley structure in the LEEM images is misleading. Bright areas indicating a high reflectivity for electrons indicate less roughened surface regions; dark areas showing a reduced reflectivity represent more strongly roughened surface area (from Ref. 15).

kept constant. The solid line in Fig. 1(a) represents the rate curve for an unfaceted Pt(110) surface. At low CO pressures, r_{CO_2} rises linearly with p_{CO}, since the O covered 1×2 surface is highly reactive. With increasing p_{CO}, the reaction rate finally drops to the low rate branch where the CO covered 1×1 surface inhibits O_2 adsorption and hence the surface reaction. Under conditions when faceting occurs, the rate does not remain stationary, but rises continuously often superimposed with transient kinetic oscillations. The rate becomes stationary again as r_{CO_2} reaches the high-rate branch, as indicated by the arrow in Fig. 1(a). The increase of the rate in time reflects the faceting of the surface which occurs within typically 10–30 min at 10^{-4} mbar. For a faceted surface, the position of the rate maximum in the r_{CO_2}, p_{CO} plot shifts towards higher p_{CO} compared to the originally flat surface, as shown by the dashed line in Fig. 1(a). It has been demonstrated by LEED and STM that faceting and roughening leads primarily to structural changes on a microscopic scale involving the range from a few to several hundred angstroms. In particular, it was shown that the facets are arranged in a regular hill and valley structure forming a sawtoothlike pattern with a lateral periodicity 150–200 Å in the $[1\bar{1}0]$ direction. Subsequent low-energy electron microscopy (LEEM) studies revealed that in addition to the microscopic structural changes also the surface topography is modified on a length scale of 0.1 to several micrometer. These macroscopic surface changes demonstrated in Figs. 1(b)–1(c) apparently result from the mass transport of Pt atoms. LEEM images of a roughened and faceted surface are shown in Figs. 1(b)–1(c).[15]

The driving force for the faceting of Pt(110) differs in its nature from a simple adsorbate-induced restructuring of the surface. Faceting is caused by the ongoing surface reaction and is not due to thermodynamical stabilization. This was demonstrated in a Monte Carlo simulation.[10] The model included probabilities for O_2 adsorption, CO adsorption, diffusion and desorption, chemical reaction, and SPT which were determined in a phenomenological way. The enhancement of O_2 adsorption at step sites was taken into account. The simulation reproduced the development of a regular facet structure with realistic time and length scales. However, this simulation was not based on a detailed atomistic description of the movement of individual Pt atoms.

To provide additional evidence that the formation of extended (100) steps on a clean Pt(110) surface is thermodynamically unfavorable, we refer to earlier experimental studies[16] detecting the ''fish scale'' pattern which exhibits a periodic island structure with extended (111) facets. The island edges are formed by single (100) steps. The periodicity of this pattern is about 1500 Å in the $[\bar{0}01]$ direction and the extension of the islands in the $[1\bar{1}0]$ direction exceeds 10000 Å. The available data[17,18] suggest that $1\times n$ superstructures, which can form in this case, are more stable than a flat 1×2 surface. The geometries exposing more extensive (111) facets are favored because the (111) structure is characterized by lower surface energy.

This communication presents a 3D kinetic Monte Carlo (KMC) model of the $CO+O_2/Pt(110)$ reaction. We start in Secs. II and III with a brief review of recently published data on CO and O_2 adsorption on different Pt surfaces. A hybrid model to be described in Sec. IV combines the KMC algorithm for SPT with a mean-field approximation for CO and O_2 adsorption on the surface. In the last sections we apply the developed model to simulate the faceting processes under various reaction conditions and compare the results with experimental measurements.

II. CO ADSORPTION ON Pt(110)

Density functional theory (DFT) calculations and experimental studies of CO adsorption under low-pressure conditions[12,13] have revealed a strong selectivity of CO adsorption with respect to different Pt surface configurations. The Pt atoms on the (110) surface are characterized by different coordination numbers n varying from 5 to 11. The values of Pt–CO binding energy $E^{Pt-CO}(n)$ at different Pt atoms vary and this dependence can be approximated by a simple linear form[12] shown in Fig. 2. The average value of $E^{Pt-CO}(n)$ is close to macroscopic data for CO desorption: $E_{des}^{CO}=-1.4$ eV (Ref. 19) and $E_{des}^{CO}=-1.651$ eV.[20]

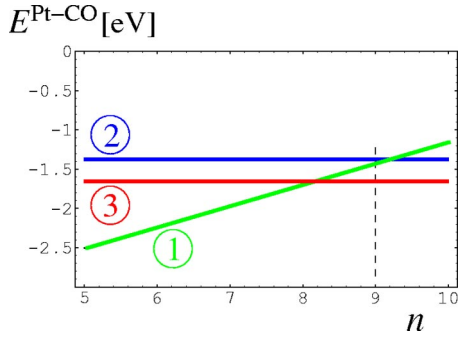

FIG. 2. Dependence of CO chemisorption energy on the coordination number of Pt atoms. The inclined line (1) is a linear fit to the data in Ref. 12; the horizontal lines (2) and (3) show the average macroscopic values of E^{Pt-CO} used in Refs. 19 and 20, respectively.

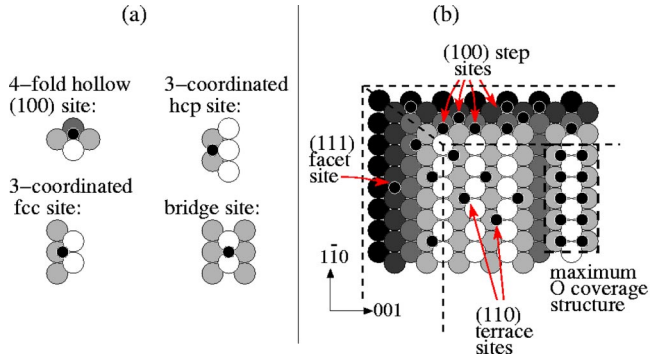

FIG. 3. (a) Ball models of different atomic configurations on Pt(110) and oxygen adsorption sites. Possible oxygen adsorption sites are indicated by small black circles. (b) (110) terraces, (100) steps, and (111) microfacets on a rough Pt(110) surface. O atoms adsorbed at fcc, hcp, and (100) step sites are shown by small black circles.

At low pressure and T>300 K, CO molecules diffuse very rapidly on the Pt(110) surface.[19] To justify this statement we consider CO diffusion between nearest neighboring (NN) atoms on a Pt(110) surface. Since the CO molecule van der Waals diameter (3.2 Å) is larger than the Pt lattice constant (2.78 Å in the [1$\bar{1}$0] direction), one can assume that CO adsorption on Pt atoms with $n>9$ is hardly possible. Also, since the number of five-coordinated atoms on the surface is extremely low (these configurations are unstable), we can assume that the highest difference in coordination between NN atoms with $n\leqslant 9$ (i.e., on which Pt–CO binding can take place) will not exceed 3. According to the linear dependence shown in Fig. 2, this difference corresponds to $\Delta E^{Pt-CO}\approx 0.8$ eV. Basically, the top layer of a 1×1 Pt(110) surface consists of seven-coordinated atoms; atoms underneath the top layer have $n=11$. The 1×2 reconstruction opens nine-coordinated atoms of (111) microfacets. In this case, ΔE^{Pt-CO} is ~0.54 eV, which is lower than activation energies for diffusion of surface Pt atoms varied within the range of 0.8–1 eV.[21–27] Note that the experimentally determined activation energies for surface diffusion of CO on Pt vary between 0.17 and 0.56 eV, with an average value being around 0.30 eV.[28,29]

III. OXYGEN ADSORPTION ON Pt(110)

Oxygen adsorption on clean Pt surfaces has been a subject of many experimental and theoretical investigations in recent years. Nanoscopic aspects, such as oxygen adsorption on Pt microfacets, diffusion of single oxygen atoms in the presence of coadsorbed CO and the influence of the adsorbate on diffusing Pt atoms have not been explored in detail although precisely these aspects might explain the development of roughening and faceting in the $CO+O_2$/Pt(110) system.

Single crystal studies[30–35] provide reliable data on oxygen sticking coefficients and adsorption rates on different Pt surfaces. Table I shows selected values of the oxygen sticking coefficients on different Pt surfaces.

Recent STM experiments and theoretical calculations demonstrated that oxygen dissociates on the Pt surface, and that the preferred sites for atomic oxygen adsorption have typically high coordination numbers. On Pt(111) oxygen occupies the threefold adsorption site, on Pt(100)-(1×1) the bridge site.[36] On a Pt(110) surface, an oxygen atom can occupy either fcc, hcp, or bridge position, as shown in Fig. 3(a).[37] Selected values of oxygen chemisorption energy on different Pt surfaces are summarized in Table II, where E^{Pt-O} values are calculated per one O atom. The theoretical calculations differ in their quantitative results for Pt(110). According to Ref. 37, the lowest energy adsorption site on Pt(110) is found to be the fcc site. The oxygen binding energy on the fcc site depends on the oxygen coverage and can vary from −3.91 eV for low coverages to −3.8 eV for the maximum coverage of the surface. At the same time, the saddle-point bridge site with an adsorption energy −3.87 eV is slightly preferred over the hcp sites with −3.7 eV. Saturation of the 1×2 surface [1 ML (monolayer) with respect to the unreconstructed 1×1 surface] is achieved when each top atom of the Pt(110) rows has four oxygen atoms adsorbed on adjacent

TABLE I. Oxygen sticking coefficients s_{O_2} on different Pt surfaces.

Surface	s_{O_2}	References
Pt(100) hex	10^{-4}–10^{-3}	30, 31
Pt(100) 1×1	0.2–0.5	30, 31
Pt(110)−1×2	0.3	32
Pt(110)−1×1	0.4–0.6	32
Pt(111)	0.06 (300 K), 0.025 (600 K)	33

TABLE II. Calculated oxygen binding energies on different Pt surfaces.

Surface	$-E^{Pt-O}$ (eV)	References	O site	Method
Pt(100)	4.587/3.155	36	fourfold hollow	LDA[a]/GGA[b]
	5.129/3.809	36	Bridge	LDA/GGA
Pt(110)	3.91/2.81	37, 38	fcc	DFT
	3.7/3.0	37, 38	hcp	DFT
	3.87/4.0	37, 38	Bridge	DFT
Pt(111)	4.9–5.87	39	Step sites	LDA

[a]Local-density approximation.
[b]Generalized gradient approximation.

fcc sites, as shown in Fig. 3(b). In contrast, the results of DFT calculations presented in Ref. 38 show an opposing tendency: the bridge sites are preferred to the hcp and fcc sites by 1 eV and more, as shown in Table II.

Following the rule of high-coordination preference for atomic adsorbates, one should expect that at (100) steps the preferred oxygen adsorption site should be the fourfold hollow position. Nevertheless, the calculated binding energies of oxygen on Pt(100) presented in Ref. 36 show that the most favorable adsorption site is the bridge site, whereas the fourfold hollow site is characterized by a slightly smaller adsorption energy.

In the case of catalytic CO oxidation on Pt(110) the reaction never formed extended Pt(100) areas but only (100) steps or (100) microfacets with a size below the detection limit of LEED. For these step sites it has been assumed that atomic oxygen adsorbs preferably at the fourfold hollow sites.

Studies of oxygen adsorption on the close-packed Pt(111) surface revealed oxygen saturation at about 0.25 ML at low oxygen partial pressures ($p_{O_2} < 1\times10^{-4}$ mbar).[39] STM observations[39] show that O atoms prefer step sites to (110) terraces on Pt(111) islands. It has also been found that O–O repulsion on the Pt(111) surface is stronger than that on Pt(110) since a close-packed hexagonal configuration of the Pt(111) surface provides smaller distances between neighboring threefold sites. The Pt–O chemisorption energy on Pt(111) reaches ~ -5.0 eV (see Table II). As in the case for (100) microfacets, oscillations, and kinetic instabilities in the $CO+O_2/Pt(110)$ system never caused formation of large (111) areas.

IV. HYBRID MODEL

A. Concept of the simulation

In order to make a complex problem such as the restructuring of a surface under catalytic conditions tractable, the system has to be simplified as far as possible. The first step consists of separating the processes in the adsorbate layer from the substrate changes. Instead of keeping track of individual CO molecules and individual oxygen atoms we treat the adsorbates as mean-field variables averaging over the whole surface area or part of it. For the surface reaction we therefore use ordinary differential equations (ODEs) based on the Langmuir-Hinshelwood scheme of catalytic CO oxidation. In contrast, for the substrate part we employ a kinetic Monte Carlo scheme to mimic the motion of individual surface Pt atoms. The two parts are coupled together, first, because the adsorbate coverages influence the surface diffusion of the Pt atoms stabilizing or destabilizing certain structural elements. Second, the restructuring of the surface will change the reactivity of the surface which enters the mean-field equations through a change of the appropriate constants. On Pt surfaces oxygen adsorption is known to be highly structure sensitive whereas CO adsorption is rather insensitive to structural modifications.

As discussed in Sec. II, equilibrium CO distribution is achieved rapidly due to high diffusivity of CO molecules between NN surface atoms. The equilibrium distribution can be approximated by a system of ODEs describing CO coverages on different surface configurations. This approach was proposed in our recent publication[40] and compared with the simplified model replacing the linear dependence of $E^{Pt-CO}(n)$ by a constant average value of the CO chemisorption energy. In the present study, we also use a single equation for CO. We make such a simplification because this model is based on reliable macroscopic data[19] and reproduces dynamics of the SPT on a realistic time scale. Moreover, the faceting and also rate oscillations take place under conditions where oxygen adsorption is rate limiting. The oxygen sticking coefficient is the most important quantity controlling the catalytic activity of the surface. This quantity varies as the surface undergoes restructuring.

One particular important structural change is the $1\times2 \rightleftharpoons 1\times1$ transition which has been shown to be responsible for the kinetic instabilities trough the different oxygen sticking coefficients that are associated with the two surface phases.[41] The SPT is also the main source for reaction-induced roughening/faceting because it is associated with the mass transport of 50% of the surface Pt atoms. Clearly the modeling of the SPT of Pt(110) is the essential part of the whole simulation. The modeling of the SPT transition of Pt(110) with the present model has already been demonstrated in the preceding paper.[40]

Since we do not restrict the motion of surface Pt atoms, in principle all possible crystallographic orientations can develop from our starting point of a flat Pt(110) surface. In practice, the low-index planes will be dominant because their higher thermodynamic stability is incorporated via corresponding jump probabilities in the simulation. Neglecting atomic-scale roughness we divide the model surface into only three types of microfacets, (100), (110), and (111) with the (110) microfacets being further subdivided into nonreconstructed (1×1) and (1×2) reconstructed area. The hex reconstruction of (100) facets is not taken into account because this reconstruction requires extended (100) facets whereas in the experiment we only observe (100) steps which presumable are single height steps.

At a temperature of 500 K, an adsorbed CO molecule is estimated to make about 3×10^9 hops per second, an oxygen atom about 16 hops per second assuming a frequency factor of $10^{13}\,s^{-1}$ and activation energies for adsorbate diffusion of 8 kcal/mol (0.35 eV) and 27 kcal/mol (1.17 eV), respectively.[29] Oxygen diffusion due to the higher binding energy is much slower than CO diffusion. Perfect mixing will not occur over the model surface area but within a microfacet which only has the dimensions of a few lattice constants mixing will still occur. The three different types of microfacets, (100), (110), and (111) will differ in their reactivity and we take this into account by following the oxygen coverages separately for each type of microfacet.

B. Definition of coverages and adsorption sites

In our model, we do not keep track of single CO molecules or O atoms, but describe the adsorbates on different surface areas as mean-field variables, i.e., coverages governed by Langmuir-Hinshelwood (LH) type equations. The adsorbate coverage θ, or absolute coverage, is given by the

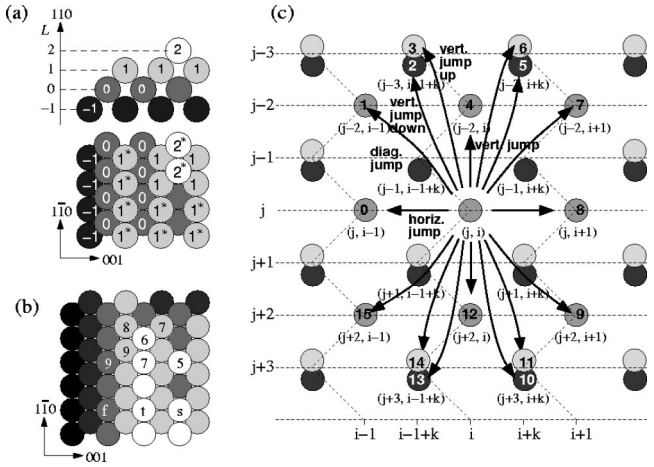

FIG. 4. Representation of the Pt(110) surface. (a) The surface relief is characterized by the matrix of heights of top sites (integer numbers, L). Free top atoms marked by an asterisk are allowed to move. (b) A model showing coordination numbers of different atomic configurations and three basic types of surface atoms. (111) facets, (110) terraces, and (100) steps are marked by "*f*," "*t*," and "s," respectively. (c) A scheme of the surface site labeling. The index shift k is introduced in order to distinguish between positions on the same layer and layers above/below; $k=j-2\,\mathrm{Int}(j/2)=\{0,\text{for even } j;1,\text{for odd } j\}$. All possible atomic jumps are shown. For a given atom $\{j,i\}$, 16 new possible positions are determined by combination of indices.

number of adsorbate atoms/molecules divided by the total number of substrate atoms of the surface. We, however, do not include explicitly the number of adparticles because such a detailed definition of the coverage matches a macroscopic value of θ defined by LH equations. Defining absolute CO coverage θ_{CO} we "average" over the whole surface area. For the oxygen coverages we distinguish between three different types of surface orientations: (100), (110), and (111). Thus, for oxygen adsorbed on (110) terraces, (100) and (111) sites we obtain $\theta_{\mathrm{O}}^{110}$, $\theta_{\mathrm{O}}^{100}$, and $\theta_{\mathrm{O}}^{111}$, respectively. Averaged over the whole surface area, these variables denote surface fractions of the respective orientations covered by oxygen.

By our definition, the top layer of the (110) surface consists of $N_{\mathrm{tot}}=2N^2$ atoms,[40,42,43] where N stands for the number of atoms in the topmost layer. Each of the surface atoms is marked by an integer L defining the upper occupied level, as shown in Fig. 4(a). We consider two atomic layers of Pt(1$\bar{1}$0) shifted by half a lattice spacing in the [001] and [1$\bar{1}$0] directions. Different surface atomic configurations are illustrated by a model in Fig. 4(b). We define a (1$\bar{1}$0) terrace site as a top surface atom bonded to the two [1$\bar{1}$0] NN atoms, i.e., when $L_{j,i}=L_{j-2,i}=L_{j+2,i}$, according to the labeling shown in Fig. 4(c). Similarly, a (100) step site is defined as a top surface atom which has only one of the two [1$\bar{1}$0] NN atoms, i.e., when $L_{j,i}=L_{j-2,i}=L_{j+2,i}+2$ or $L_{j,i}=L_{j+2,i}=L_{j-2,i}+2$. A surface atom with coordination number $n=9$, which is covered by two NN atoms in the higher layer, may form a (111) site if the following condition is fulfilled: $L_{j,i}=L_{j,i-1}+2=L_{j,i+1}-2$ or $L_{j,i}=L_{j,i-1}-2=L_{j,i+1}+2$. Coordination numbers of the surface atoms are determined in a similar way: for each coordination, a unique relation for heights of NN atoms can be written according to Figs. 4(b) and 4(c).

To evaluate the surface fraction of sites available for CO adsorption x_{CO} (or maximum CO coverage), we determine the number of Pt atoms with coordination number $5\leqslant n\leqslant 9$ (N_{5-9}). Then we define

$$x_{\mathrm{CO}}=2N_{5-9}/N_{\mathrm{tot}}$$

with $x_{\mathrm{CO}}=0.5$ for the 1×2 surface and $x_{\mathrm{CO}}=1$ for the 1×1 state. Note that at CO saturation ($\theta_{\mathrm{CO}}=1$), the surface has a close-packed 1×1 structure and $N_{5-9}=N_7=N^2$.

The surface fractions of sites available for oxygen adsorption on (110) terraces, (100) and (111) sites are given as

$$x_{\mathrm{O}}^{110}=\alpha_{110}N_{110}/N_{\mathrm{tot}},\quad x_{\mathrm{O}}^{100}=\alpha_{100}N_{100}/N_{\mathrm{tot}},$$

$$x_{\mathrm{O}}^{111}=\alpha_{111}N_{111}/N_{\mathrm{tot}},$$

where N_{110}, N_{100}, and N_{111} are the numbers of Pt atoms forming (110), (100), and (111) sites, as shown in Fig. 4(b), and the coefficients α_{110}, α_{100}, and α_{111} denote the numbers of oxygen adsorption sites per Pt atom on (110) terraces, and (100) and (111) surface areas, respectively. We assume that there are maximum two adjacent fcc (hcp) positions per each terrace atom (according to Fig. 3), i.e., $\alpha_{110}=2$. Thus, $x_{\mathrm{O}}^{110}=0.5$ for the 1×2 surface and $x_{\mathrm{O}}^{110}=1$ for the 1×1 state. To evaluate the number of (100) step sites we take into account Pt atoms which have only one of the two [1$\bar{1}$0] NN atoms, i.e., there is only one fourfold hollow position corresponding to each (100) step atom; therefore we define $\alpha_{100}=1$. We also assume that $\alpha_{111}\ll1$ due to strong O–O repulsive interactions on the (111) surface.

We also define relative coverages as

$$y_{\mathrm{CO}}=\theta_{\mathrm{CO}}/x_{\mathrm{CO}},\quad y_{\mathrm{O}}^{110}=\theta_{\mathrm{O}}^{110}/x_{\mathrm{O}}^{110},$$

$$y_{\mathrm{O}}^{100}=\theta_{\mathrm{O}}^{100}/x_{\mathrm{O}}^{100},\quad y_{\mathrm{O}}^{111}=\theta_{\mathrm{O}}^{111}/x_{\mathrm{O}}^{111},$$

where y_{CO} stands for the relative coverage of CO averaged over the surface sites with coordination numbers $5\leqslant n\leqslant9$ and y_{O}^{110}, y_{O}^{100}, and y_{O}^{111} denote the relative coverages of oxygen averaged over (110), (100), and (111) sites, respectively. These coverages vary when the surface undergoes restructuring even if the number of adparticles remains the same. Since nanodomains of different surface orientations are present on a roughened surface the relative coverages become in principle local variables.

C. A mean-field equations

Our choice of kinetic equations is motivated in Sec. IV A. The following set of equations is used in our simulations (Reichert *et al.*[19]), which were shown to correctly reproduce the essential experimental data for Pt(110)/CO $+\mathrm{O}_2$:

$$\frac{\partial\theta_{\mathrm{CO}}}{\partial t}=p_{\mathrm{CO}}k_{\mathrm{CO}}^{ad}s_{\mathrm{CO}}(1-y_{\mathrm{CO}})-k_{\mathrm{CO}}^{des}\theta_{\mathrm{CO}}-\theta_{\mathrm{CO}}(k_r^{110}\theta_{\mathrm{O}}^{110}+k_r^{100}\theta_{\mathrm{O}}^{100}+k_r^{111}\theta_{\mathrm{O}}^{111}),\tag{1}$$

$$\frac{\partial\theta_{\mathrm{O}}^{110}}{\partial t}=p_{\mathrm{O}_2}k_{\mathrm{O}_2,110}^{ad}s_{\mathrm{O}_2}^{110}(1-y_{\mathrm{CO}})^2(1-y_{\mathrm{O}}^{110})^2-k_r^{110}\theta_{\mathrm{CO}}\theta_{\mathrm{O}}^{110},\tag{2}$$

$$\frac{\partial \theta_O^{100}}{\partial t} = p_{O_2} k_{O_{2,100}}^{ad} s_{O_2}^{100} (1-y_{CO})^2 (1-y_O^{100})^2 - k_r^{100} \theta_{CO} \theta_O^{100}, \quad (3)$$

$$\frac{\partial \theta_O^{111}}{\partial t} = p_{O_2} k_{O_{2,111}}^{ad} s_{O_2}^{111} (1-y_{CO})^2 (1-y_O^{111})^2 - k_r^{111} \theta_{CO} \theta_O^{111}. \quad (4)$$

The variables used in Eqs. (1)–(4) are described in Sec. IV B and kinetic parameters are introduced in Sec. IV D. It should be noted that the equations for the adsorbates are coupled to the substrate lattice via the corresponding fractions of the adsorption sites which vary depending on the degree of roughening/faceting of the substrate. Integration of Eqs. (1)–(4) has been carried out by a Runge-Kutta scheme after each Monte Carlo step (see Sec. IV E and the Appendix for details on Monte Carlo procedure).

Because CO and oxygen adsorption sites are not identical, the inhibition of oxygen and CO adsorption by adsorbates is not symmetrical. CO molecules adsorb atop of Pt atoms, whereas atomic oxygen occupies fcc/hcp/(100) positions, CO adsorption may therefore take place even on an fully oxygen covered surface. Accordingly the CO adsorption rate in Eq. (1) is only proportional to $(1-y_{CO})$. The dissociative adsorption of an oxygen molecule takes place if (i) two neighboring bridge sites are not occupied by CO molecules and (ii) two adjacent fcc/hcp/(100) sites are free of O. Thus, the oxygen adsorption rates in Eqs. (2)–(4) are proportional to $(1-y_{CO})^2(1-y_O)^2$.

We assume that (110) terrace sites can be transformed by roughening/faceting into (100) step sites and vice versa. This change in the substrate, in turn, leads to an increase or decrease of the relative coverages on the different microfacet orientations. In the computation we proceed as follows. If at some time step θ_i exceeds x_i due to a sharp decrease of x_i, we define $\theta_i = x_i$ on the next time step, where $i =$ ''CO'' or ''O.'' If the integration time is small, this will not introduce an essential numerical error in the simulation. We also note that Eqs. (1)–(4) do not include an adsorbate exchange between different adsorption sites. Such an assumption allowing the equilibrium distribution of the adsorbates during a one Monte Carlo step should not affect accuracy of the simulation.

D. Choice of kinetic constants

We define the oxygen sticking coefficients $s_{O_2}^{110}$, $s_{O_2}^{100}$, and $s_{O_2}^{111}$ in the following form (in accordance with Table I):

$$s_{O_2}^{110} = 0.6 x_{110} = \begin{cases} 0.3 & \text{on} \quad 1\times 2 \\ 0.6 & \text{on} \quad 1\times 1, \end{cases} \quad (5)$$

$$s_{O_2}^{100} = 1.0 x_{100}, \quad (6)$$

$$s_{O_2}^{111} = 0.05 x_{111}. \quad (7)$$

It should be noted, however, that experimentally measured sticking coefficients are in generally only available for macroscopic crystal planes but not for isolated single step sites. Moreover, a s_{O_2} value determined for a perfect single crystalline Pt surface may not be equal to that of a microfacet of the same surface orientation due to size effects.

TABLE III. Kinetic parameters used in the model (from Ref. 19).

Sticking coefficients		
CO adsorption:	s_{CO}	1
O_2 adsorption:	$s_{O_2}^{110}$, $s_{O_2}^{100}$, $s_{O_2}^{111}$	Eqs. (5)–(7)
Arrhenius rates		$\nu \exp(-E/RT)$
CO desorption:	k_{des}^{CO}	$\nu_{des} = 5\times 10^{13}\ s^{-1}$, $E_{des} = 32.3$ kcal/mol (or 1.4 eV)
CO+O reaction:	k_r	$\nu_r = 5\times 10^5\ s^{-1}$, $E_r = 8.1$ kcal/mol

The experimental data suggest clearly that the oxygen sticking coefficient on (100) steps is higher than $s_{O_2}^{110}$ and $s_{O_2}^{111}$.[4–10] For the sake of simplicity, we assume that the sticking probability of O_2 on (100) steps equals to 1. Apparently the behavior of (100) steps is quite different from that of an extended (100) facet. For the latter, depending on whether the facet is in a 1×1 configuration or hex reconstructed, the sticking coefficient is lower than on Pt(110).

The kinetic parameters used in our model are listed in Table III. For simplicity, we assume that the oxygen impingement rate constant $k_{O_2}^{ad}$ is constant irrespective of the degree of roughening/faceting. The surface reaction constants on terraces, (100) and (111) sites are also assumed to be equal to the average value k_r estimated for Pt(110).[19] Since the simulations show that the oxygen coverage of (111) microfacets is insignificant compared to that of (110) terraces and (100) microfacets, we can drop Eq. (4).

E. Kinetic Monte Carlo model

In the substrate part we employ kinetic MC to simulate the movement of Pt atoms on a catalytically active surface. Pt atoms can change their position due to activated thermal movement but the jump probability depends on the relative adsorbate coverage. The adsorbates changes the binding energy of the Pt atom to which an adsorbate atom/molecule is bonded as well as the activation barrier for the movement of the Pt atom. Since the higher CO adsorption energy of CO on the 1×1 phase is the driving force for the CO-induced lifting of the 1×2 reconstruction, the $1\times 2 \rightleftharpoons 1\times 1$ phase transition is incorporated in the model via the corresponding jump probabilities of Pt atoms.

Assuming that the population of adsorption sites occurs according to thermodynamical equilibrium we can calculate occupation probabilities for individual adsorption sites based on a Boltzmann distribution.

KMC computations involve single jumps of Pt atoms to vacant neighboring positions. Only five kinds of paths will be allowed: parallel and perpendicular to the $[1\,1\,0]$ direction (called, respectively, ''vertical'' and ''horizontal''), diagonal and hopping up or down via the leapfrog (LF) mechanism.[21–27] We do not consider explicitly long jumps

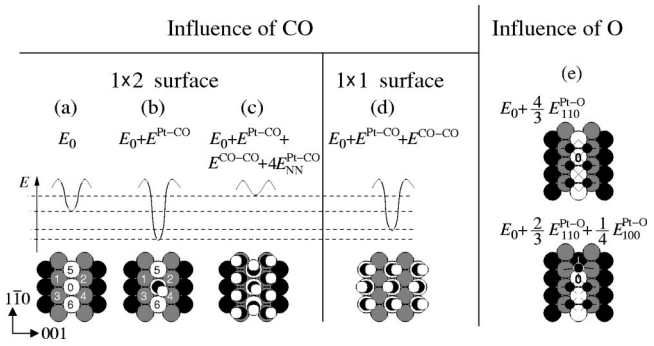

FIG. 5. Modification of the surface energy due to the adsorbates. The first four panels (a)–(d) show relative energy levels for a clean 1×2 surface and different CO covered 1×2 and 1×1 states. Small double black-white circles denote CO molecules. (a) The central Pt atom (0) on a clean 1×2 surface has the energy E_0. (b) A CO molecule attached atop this atom decreases its energy by adding $E^{Pt-CO}<0$. (c) Further adsorption of CO on the lower atomic layer [sites (1)–(4)] destabilizes the central atom ($4E^{Pt-CO}_{NN}>0$ is added). CO molecules adsorbed on the NN sites 5 and 6 interact with CO attached atop the central atom ($E^{CO-CO}>0$ is added). (d) A CO saturated 1×1 surface is more stable than the states shown in panels (a) and (c), since there is no CO adsorption on sites 1–4. (e) Oxygen atoms adsorbed on fcc and (100) sites modify the energy by adding $E^{Pt-O}_{110}<0$ and $E^{Pt-O}_{100}<0$ (the respective energy of the central Pt atom (0) is presented); O atoms are shown by small black circles.

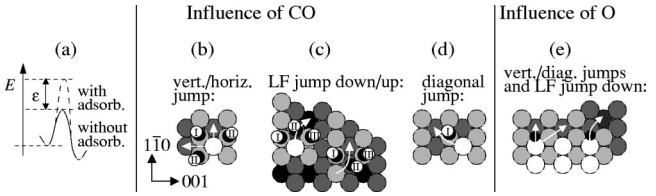

FIG. 6. Modification of the activation barriers due to CO and O_2 adsorption. (a) Schematic increase of the transition state energy. (b) The vertically/horizontally hopping Pt atom may interact with two CO molecules marked by I and II. (c) The LF hopping can be inhibited by three CO molecules attached to adjacent sites marked by I, II, and III. (d) The diagonal jump can be inhibited by a one CO molecule (marked by I). (e) Jumps of a step atom are restricted by repulsive interactions with O atoms attached to the fourfold positions. O atoms are shown by small black circles.

and diffusion of atomic clusters, which, however, can be effected through combination of the allowed elementary steps. The diagonal jump can be introduced instead of a displacement via an exchange mechanism.[27] We assume the energy of a Pt surface atom to be dependent on the Pt occupancy of the four adjacent sites in the same layer and to be modified by CO and oxygen adsorption. The modification of the surface energy by CO and atomic oxygen is shown schematically in Fig. 5. On completely CO covered 1×2 patches of the surface, the modified energy of a Pt atom can be expressed in the following form [in accordance with Fig. 5(c)],

$$E=E_0+E^{\mathrm{Pt-CO}}(n)+4E^{\mathrm{Pt-CO}}_{\mathrm{NN}}+E^{\mathrm{CO-CO}}, \tag{8}$$

where the energy of a Pt atom on a clean surface is determined as $E_0=n_vE_v+n_hE_h$ with n_v, n_h denoting the numbers of Pt-occupied vertical $[1\bar{1}0]$ and horizontal [001] positions in the same layer and E_v, E_h denoting the Pt–Pt binding energies between the adjacent atoms; $E^{\mathrm{Pt-CO}}_{\mathrm{NN}}$ is the repulsive interaction energy between the central Pt atom (0) and CO molecules adsorbed on the NN positions in the layer below (1–4); $E^{\mathrm{CO-CO}}$ is the repulsive interaction energy between CO molecules attached to the Pt atom (0) and its adjacent sites (5,6). It should be noted, however, that the CO covered 1×2 state according to Eq. (8) and Fig. 5(c) is unstable due to strong repulsive interactions between the central Pt atom (0) and CO molecules attached to the (1–4) sites ($E^{\mathrm{Pt-CO}}_{\mathrm{NN}}>0$).

The energy of a top Pt atom on the O covered surface can be defined according to Fig. 5(e) as follows:

$$E=E_0+\begin{cases}\frac{4}{3}E^{\mathrm{Pt-O}}_{110} & \text{on terraces}\\ \frac{2}{3}E^{\mathrm{Pt-O}}_{110}+\frac{1}{4}E^{\mathrm{Pt-O}}_{100} & \text{on (100) steps,}\end{cases} \tag{9}$$

where $E^{\mathrm{Pt-O}}_{110}$ and $E^{\mathrm{Pt-O}}_{100}$ are average O chemisorption energies at threefold terrace sites (fcc) and fourfold (100) step positions, respectively. We neglect O_2 adsorption on (111) microfacets of the surface.

The adsorbate modification of activation barriers for Pt atom jumps can be taken into account in a similar way: CO molecules adsorbed on the sites which are adjacent to the path of the migrating Pt atom increase the energy of transition state, as shown schematically in Fig. 6(a). Since the CO molecule van der Waals diameter is larger than the Pt lattice constant, diffusing Pt atoms cannot avoid interactions with CO molecules. As illustrated in Fig. 6(b), the displacements along or across $[1\bar{1}0]$ direction may be inhibited by two CO molecules adsorbed on the two NN sites on the layer below (marked by I and II in the figure). The LF hopping can be inhibited by the CO adsorption on the three adjacent sites (I,II,III) as shown in Fig. 6(c), whereas the atom hopping in the diagonal way may interact with only one CO molecule [see Fig. 6(d)]. Thus, we define the increase of activation barrier E^a_i of the vertical, horizontal, diagonal, and LF jumps on the CO covered surface, according to Figs. 6(b)–6(d), as

$$E^a_i=\begin{cases}E^0_{\mathrm{vert/horiz}}+2\epsilon^{\mathrm{Pt-CO}}\\ E^0_{\mathrm{diag}}+\epsilon^{\mathrm{Pt-CO}}\\ E^0_{\mathrm{LF}}+3\epsilon^{\mathrm{Pt-CO,}}\end{cases} \tag{10}$$

where $E^0_{\mathrm{vert/horiz}}$, E^0_{diag}, and E^0_{LF} are the transition state energies of Pt atom on a clean Pt(110) surface and $\epsilon^{\mathrm{Pt-CO}}$ is the correction modeling repulsive interaction between the Pt atom and CO molecules adsorbed on the adjacent sites.

We also assume that atomic oxygen will stabilize the (100) steps by increasing the activation barriers for the vertical and diagonal jumps and the LF hopping down of the step atoms, as shown in Fig. 6(e). The transition state energy on the oxygen covered surface can be defined as

$$E^a_i=E^0_i+\epsilon^{\mathrm{Pt-O}}_i, \tag{11}$$

where the index i stands for the vertical and diagonal displacements and LF hopping down, and $\epsilon^{\mathrm{Pt-O}}_i$ is the correction modeling the increase of transition state energy due to an oxygen atom attached to the fourfold (100) step position. The oxygen atoms adsorbed on terraces can easily switch be-

tween fcc and hcp sites. Oxygen atoms are relatively small and, therefore, the O binding at fcc positions will not restrict horizontal displacement of terrace Pt atoms.

The rate of a single atomic step (hopping) on a clean surface is expressed in the Arrhenius form,

$$r_i = \nu_h \exp(-\Delta E_i / k_B T), \tag{12}$$

where $\Delta E_i = E_i^a - E_0$ is the activation barrier of ith hopping and $i =$ ''vert,'' ''hor,'' ''diag,'' ''LF-up'' or ''LF-down.'' Each hopping event on the surface occurs on the average once in the time interval $t_i = 1/r_i$. The characteristic time of the fastest step $\Delta t = 1/r_{\max} = 1/r(\Delta E_{\min})$ can be identified with a Monte Carlo step (MCS), i.e., the number of attempts equal to the surface lattice dimension. This allows us to translate MC units to real time and probabilities of MC jumps to actual reaction rates. The probability of an atomic step P_i is defined as

$$P_i = r_i / r_{\max} = t_{\min} / t_i = \exp[-(\Delta E_i - \Delta E_{\min})/k_B T]. \tag{13}$$

This means that each free atom on the surface lattice moves on the average once via the ith path with the probability P_i during the physical time interval Δt.

We define a correction to the transition probability arising due to interactions with an adsorbate as a multiplying factor, which is equal to 1 for the adsorbate-free configuration ($\theta_{\mathrm{CO}} = 0$ or $\theta_{\mathrm{O}} = 0$) and $\exp(\mathcal{H}/k_B T)$ for the adsorbate covered state ($\theta_{\mathrm{CO}} = 1$ or $\theta_{\mathrm{O}} = 1$) with $\mathcal{H}$ modeling the modification of the energy or activation barrier ($\mathcal{H}$ may be positive or negative depending on the interaction type). According to Figs. 5(a)–5(d), the corrections to the atomic surface energy arising due to CO adsorption on the (0–6) sites are taken into account in the following way:

$$p_1 = (1-\theta_0) + \theta_0 \exp[E^{\mathrm{Pt-CO}}(n)/k_B T], \tag{14}$$

$$\begin{aligned} p_2 = {} & \prod_{i=1}^{4} \theta_i \exp(4E_{\mathrm{NN}}^{\mathrm{Pt-CO}}/k_B T) + \sum_{i=1}^{4} \left((1-\theta_i) \prod_{j=1, j\neq i}^{4} \theta_j \right) \\ & \times \exp(3E_{\mathrm{NN}}^{\mathrm{Pt-CO}}/k_B T) + \sum_{i=1}^{4} \sum_{j=i+1}^{4} \left((1-\theta_i)(1-\theta_j) \right. \\ & \left. \times \prod_{k=1, k\neq i, k\neq j}^{4} \theta_k \right) \exp(2E_{\mathrm{NN}}^{\mathrm{Pt-CO}}/k_B T) \\ & + \sum_{i=1}^{4} \left(\theta_i \prod_{j=1, j\neq i}^{4} (1-\theta_j) \right) \exp(E_{\mathrm{NN}}^{\mathrm{Pt-CO}}/k_B T) \\ & + \prod_{i=1}^{4} (1-\theta_i), \end{aligned} \tag{15}$$

$$p_3 = (1 - \theta_0\theta_5\theta_6) + \theta_0\theta_5\theta_6 \exp(E^{\mathrm{CO-CO}}/k_B T), \tag{16}$$

$$p^{\mathrm{CO}} = p_1 p_2 p_3, \tag{17}$$

where $\theta_l = y_{\mathrm{CO}}(n)$, the index l runs from 0 to 6 and labels the NN atoms with the coordination number n. These expressions have been obtained for intermediate coverages $[0 \leqslant \theta_{\mathrm{CO}}(n) \leqslant 1]$. The correction to the transition probability due to modification of the energy of terrace and (100) step atoms by adsorbed oxygen is expressed in the following form:

$$p^{\mathrm{O}} = (1 - y_{\mathrm{O}}^{110}) + y_{\mathrm{O}}^{110} e^{((4/3)E_{110}^{\mathrm{Pt-O}})/k_B T} \tag{18}$$

on terraces or

$$\begin{aligned} p^{\mathrm{O}} = {} & (1-y_{\mathrm{O}}^{110})(1-y_{\mathrm{O}}^{100}) + y_{\mathrm{O}}^{110}(1-y_{\mathrm{O}}^{100}) e^{((2/3)E_{110}^{\mathrm{Pt-O}})/k_B T} \\ & + y_{\mathrm{O}}^{100}(1-y_{\mathrm{O}}^{110}) e^{((1/4)E_{100}^{\mathrm{Pt-O}})/k_B T} \\ & + y_{\mathrm{O}}^{110} y_{\mathrm{O}}^{100} e^{((2/3)E_{110}^{\mathrm{Pt-O}} + (1/4)E_{100}^{\mathrm{Pt-O}})/k_B T} \end{aligned} \tag{19}$$

on (100) steps.

Similarly, one can derive the corrections to activation barriers on CO and O covered surfaces, respectively. The following CO modifications have been included for vertical or *horizontal* displacement:

$$\begin{aligned} b_{\mathrm{CO}} = {} & \theta_{\mathrm{I}}\theta_{\mathrm{II}} \exp(2\epsilon^{\mathrm{Pt-CO}}/k_B T) + [\theta_{\mathrm{I}}(1-\theta_{\mathrm{II}}) + (1-\theta_{\mathrm{I}})\theta_{\mathrm{II}}] \\ & \times \exp(\epsilon^{\mathrm{Pt-CO}}/k_B T) + (1-\theta_{\mathrm{I}})(1-\theta_{\mathrm{II}}), \end{aligned} \tag{20}$$

diagonal displacement:

$$b_{\mathrm{CO}} = (1-\theta_{\mathrm{I}}) + \theta_{\mathrm{I}} \exp(\epsilon^{\mathrm{Pt-CO}}/k_B T), \tag{21}$$

and vertical *jump up/down* to the layer above/below (LF):

$$\begin{aligned} b_{\mathrm{CO}} = {} & \prod_{i=1}^{\mathrm{III}} \theta_i \exp(3\epsilon^{\mathrm{Pt-CO}}/k_B T) \\ & + \sum_{i=1}^{\mathrm{III}} \left[(1-\theta_i) \prod_{j=1, j\neq i}^{\mathrm{III}} \theta_j \right] \exp(2\epsilon^{\mathrm{Pt-CO}}/k_B T) \\ & + \sum_{i=1}^{\mathrm{III}} \left[\theta_i \prod_{j=1, j\neq i}^{\mathrm{III}} (1-\theta_j) \right] \exp(\epsilon^{\mathrm{Pt-CO}}/k_B T) \\ & + \prod_{i=1}^{\mathrm{III}} (1-\theta_i), \end{aligned} \tag{22}$$

where $\theta_l = y_{\mathrm{CO}}(n)$ and the sites are numbered ($l =$ I, II, or III) according to Fig. 6(b). For the *hopping of the (100) step atom* on an O covered surface configuration the correction reads

$$b_{\mathrm{O}} = (1 - y_{\mathrm{O}}^{100}) + y_{\mathrm{O}}^{100} \exp(\epsilon_i^{\mathrm{Pt-O}}/k_B T), \tag{23}$$

where $i =$ vert, diag, and LF-down.

The final form of the transition probability reads

$$P_i = \exp\left(-\frac{\Delta E_i - \Delta E_{\min}}{k_B T} \right) (p^{\mathrm{CO}} p^{\mathrm{O}})(b_{\mathrm{CO}} b_{\mathrm{O}})^{-1}. \tag{24}$$

It should be noted that in limiting cases the transition probability has a conventional form: for θ_{CO}, $\theta_{\mathrm{O}}^{110}$, $\theta_{\mathrm{O}}^{100} = 0$, the value of P_i is defined by Eq. (13). In the case of full CO saturation (i.e., the unstable CO covered 1×2 state), P_i includes the activation barrier $\Delta E_i = E_i^a - E$ defined by Eqs. (8) and (10) in Eq. (13), whereas on the O saturated surface the transition probability is calculated by using Eqs. (9) and (11) in Eq. (13).

The values of KMC model parameters used in the simulations are summarized in Table IV. Details on computation of atomic jumps and the model algorithm are presented in the Appendix.

TABLE IV. KMC model parameters (hopping frequency factor $\nu_h = 10^{10.7}\,\mathrm{s}^{-1}$).

Parameter	Value (eV)	Notes and References
E_v	−0.225	12
E_h	0.05	
$E^{\mathrm{Pt-CO}}(n)$	−1.4	$5 \leqslant n \leqslant 9$, 19
$E^{\mathrm{Pt-O}}_{110}$	−3.5	37, 38
$E^{\mathrm{Pt-O}}_{100}$	−4.0	36
$E^{\mathrm{Pt-CO}}_{\mathrm{NN}}$	0.07	Fit
$E^{\mathrm{CO-CO}}$	0.03	Fit
$E^a_{\mathrm{vert}} = E^a_{\mathrm{hor}} = E^a_{\mathrm{LF\text{-}up/down}}$	0.91	Fit to Refs.: 11, 22, 23, 25, 26
E^a_{diag}	0.92	
$\epsilon^{\mathrm{Pt-CO}}$	0.07	Fit
$\epsilon^{\mathrm{Pt-O}}_{\mathrm{vert}}$	0.25	Fit
$\epsilon^{\mathrm{Pt-O}}_{\mathrm{diag}}$	0.02	Fit
$\epsilon^{\mathrm{Pt-O}}_{\mathrm{LF\text{-}down}}$	0.02	Fit
ΔE_{min}	0.81	22, monomers in 1×2 channels

V. NUMERICAL RESULTS

In Ref. 19, the following macroscopic impingement rates for oxygen and CO adsorption on Pt(110) are provided: $k^{ad}_{\mathrm{O}_2} = 5.858 \times 10^5\,\mathrm{mbar}^{-1}\,\mathrm{s}^{-1}$ and $k^{ad}_{\mathrm{CO}} = 3.135 \times 10^5\,\mathrm{mbar}^{-1}\,\mathrm{s}^{-1}$. For isolated single atomic configurations, however, the values of k^{ad}_{CO} and $k^{ad}_{\mathrm{O}_2}$ as well as the sticking coefficients may differ and exact estimation of these parameters on roughened surface is hardly possible. Oscillations and faceting occur in the system under the study only in a narrow region of the p_{CO}, p_{O_2}-parametric plane.[19,20] In principle, this region can be reproduced by our model, but numerous long run computations are required in order to adjust appropriate values of k^{ad}_{CO} and $k^{ad}_{\mathrm{O}_2}$. Therefore, we choose values of products $\alpha = k^{ad}_{\mathrm{O}_2} p_{\mathrm{O}_2}$ and $\beta = k^{ad}_{\mathrm{CO}} p_{\mathrm{CO}}$ to obtain a dynamical behavior qualitatively similar to that found in the experiment. Performing a number of simulations in the extended range of α and β one can obtain the conditions for existence of oscillations and faceting and then the appropriate values of $k^{ad}_{\mathrm{O}_2}$ and k^{ad}_{CO} can be found by simple rescaling. Exact reproduction of the oscillation diagram in p_{CO}, p_{O_2} plane, however, is out of our interest in the present work.

In Fig. 7 we plot the CO_2 production rate versus $k^{ad}_{\mathrm{CO}} p_{\mathrm{CO}}$ at fixed $k^{ad}_{\mathrm{O}_2} p_{\mathrm{O}_2}$. Figure 7 shows three different regimes corresponding to those in the experimental Fig. 1(a). The simulations have been carried out for 480 K and 520 K yielding similar results in both cases. The reaction-induced surface structures obtained under varying conditions are illustrated in Fig. 8 by simulations corresponding to regions I, II, and III in Fig. 7.

At low p_{CO} (region I in Fig. 7), a 1×2 structure characterized by small domain sizes and structural defects was obtained [as shown in Fig. 8(Ia)]. This surface state is associated with a high O coverage. An increase of p_{CO} but still within region I causes a strong roughening associated with the development (100) and (111) microfacets as shown in Fig. 8(Ib). As p_{CO} enters the region II in Fig. 7, kinetic instabilities and transient oscillations evolve. The CO_2 production rate fluctuates within the shaded area of the region II in Fig. 7.

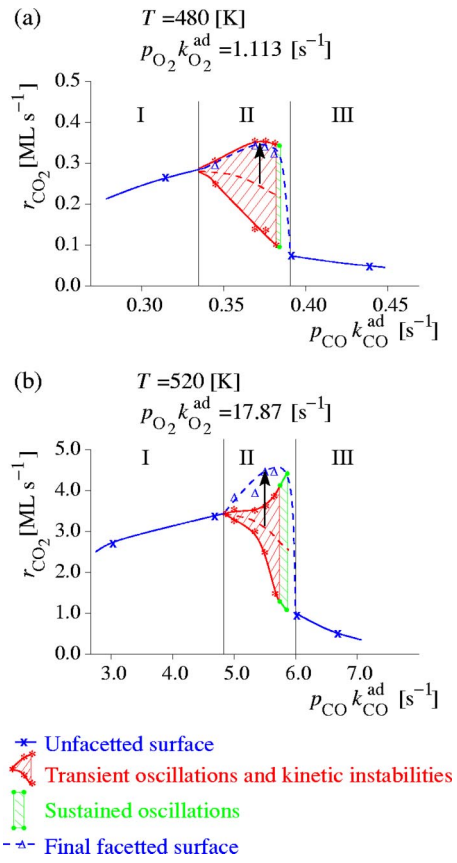

FIG. 7. Simulated diagrams of CO_2 production rate, $r_{\mathrm{CO}_2} = k_r \theta_{\mathrm{CO}} (\theta^{110}_{\mathrm{O}} + \theta^{100}_{\mathrm{O}})$, vs $p_{\mathrm{CO}} k^{ad}_{\mathrm{CO}}$ at different values of T and $p_{\mathrm{O}_2} k^{ad}_{\mathrm{O}_2}$. The O covered 1×2 roughened surface is obtained in region I. An increase of p_{CO} causes kinetic instabilities and transient oscillations. The dashed curve inside the shaded area represents the average r_{CO_2} on an unfaceted surface. Atomic transport caused by kinetic instabilities leads to a strongly faceted surface state (region II) characterized by a high r_{CO_2}. Continuous oscillations occur within a narrow region of higher p_{CO}, near the boundary of stability of the faceted state. At high p_{CO} (region III), the 1×1 state is established.

As a consequence of the CO coverage oscillations the SPT occurs quite frequently intensifying the mass transport of Pt atoms on the surface. A strongly faceted surface is generated, as displayed in Fig. 8(II); this state is stable under reaction conditions (but it is metastable without reaction). The oscillations vanish, but the rate still gradually increases until it reaches the high-rate branch where it becomes stationary. The transient oscillations of the adsorbate coverages and of r_{CO_2} during faceting are reproduced in Fig. 9. The overall growth of r_{CO_2} can be attributed to the formation of additional (100) steps during faceting. The (100) steps are characterized by a high oxygen sticking coefficient, thus, leading to an increase in catalytic activity under conditions where oxygen adsorption is rate limiting.

Finally, if p_{CO} is very high (region III in Fig. 7), a fully CO covered 1×1 structure shown in Fig. 8(III) inhibits the adsorption of O_2 and, thus, the surface reaction. No faceting can develop due to the absence of a catalytic reaction.

A regular faceted surface structure is obtained if the computations are carried out on a large lattice (2×150^2 at-

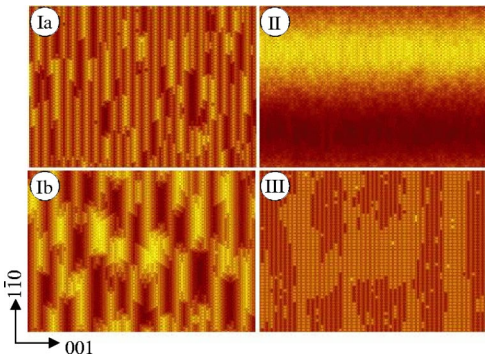

FIG. 8. Pt(110) surfaces simulated at different p_{CO} and fixed p_{O_2} corresponding to the regimes shown in Fig. 7. (Ia) The 1×2 surface obtained at low p_{CO}. (Ib) An island structure with (100) and (111) microfacets established due to an increase of p_{CO} in the region I. (II) A strongly faceted surface obtained at p_{CO} values corresponding to the region II in Fig. 7. (III) A flat 1×1 state obtained at high p_{CO} (region III in Fig. 7). The simulations have been carried out on a lattice of 2×50^2 atoms.

oms). Figure 10 shows how the surface transforms if conditions corresponding to region II are chosen. Profile cuts in the [1$\bar{1}$0] direction taken at different time moments show the development of a periodic hill and valley structure. At $t\approx3000$ s, the average inclination angle of the hills corresponds roughly to facets of (430) and (320) orientation. The atomistic structure of the faceted surface at $t=3000$ displayed in Fig. 11 shows that the slopes consist of (100) steps and (110) terrace units.

With progressing time the slopes of the facets become steeper and the structure becomes more regular. An almost perfect periodic structure is obtained at $t\approx4000$ s. Longer exposure to reaction conditions hardly affects the periodicity and the inclination angle of the hills. The atomic structure of this strongly faceted surface is shown in Fig. 11(b) displaying a fragment of the model surface at $t=9000$ s. The slope exhibit multiple height (100) steps including small patches of (210) microfacets. The periodicity of 50–60 lattice units in the [1$\bar{1}$0] direction obtained in the simulations corresponds to ~140–170 Å, which compares well with the experimental value.

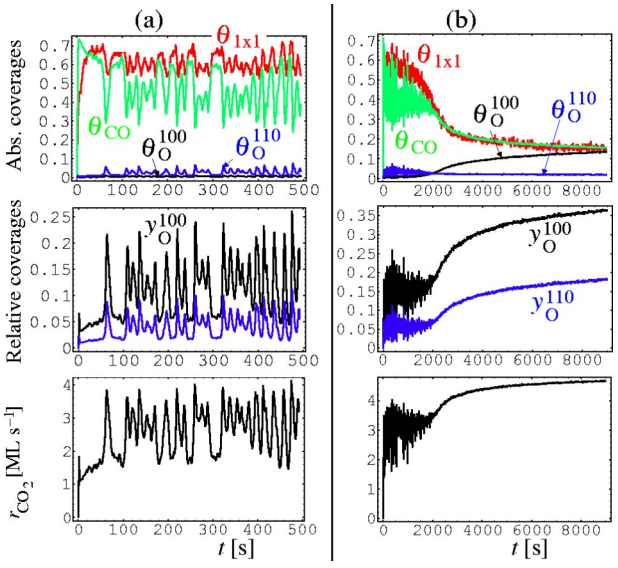

FIG. 9. Transient oscillations obtained in the simulations with the values of parameters taken from Region II in Fig. 7 and at $T=520$ K. The left column (a) shows initial oscillations ($t\leq500$ s) of the absolute and relative adsorbate coverages as well as the CO_2 production rate. The right column (b) presents relaxation to a strongly faceted O-covered state in a long run.

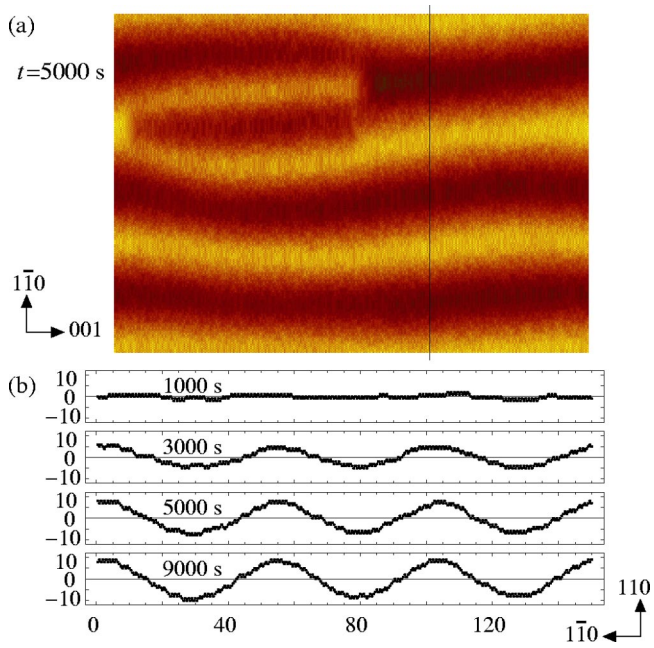

FIG. 10. (a) A simulated surface of 2×150^2 atoms showing facets which are formed by (100) steps. (b) Changes in the surface profile during the development of faceting. The surface sections at different time moments were taken in the [1$\bar{1}$0] direction as shown by the line in (a). The periodicity of 50–60 lattice units in the [1$\bar{1}$0] direction corresponds to ~140–170 Å.

A high-temperature simulation without adsorbates shows that the faceted surface smooths out rapidly at $T=700$ K. The profile cuts demonstrating this behavior are shown in Fig. 12. As an average characteristic of roughening and faceting, one can use the variance of atomic layers measuring the

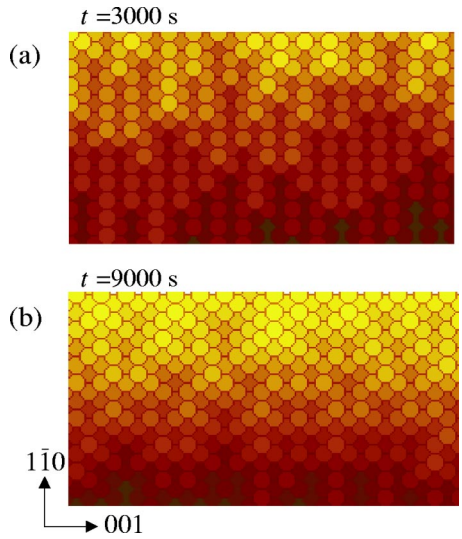

FIG. 11. Fragments of the simulated surfaces (2×150^2 atoms) captured at $t=3000$ s and $t=9000$ s. The surfaces show different angles of inclination.

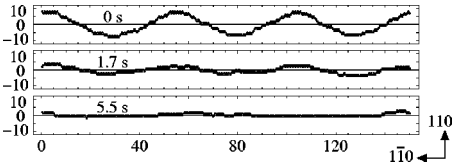

FIG. 12. Simulation of restoration of the flat surface at $T=700$ K and in the absence of adsorbates (p_{CO}, p_{O_2}, θ_{CO}, and θ_O are equal to zero). The simulation started from the periodic structure obtained at $t=5000$ s.

height dispersion of top Pt atoms. Figure 13(a) shows the variance increasing due to atomic transport caused by the kinetic instabilities. The faceted state is characterized by a higher variance of top atom layers. A rapid decrease of faceting under heating is illustrated by the variance reduction in Fig. 13(b).

In contrast to a simple model[10] mentioned in Sec. I, our KMC model cannot reproduce complete restoration of a flat surface after removing the adsorbates at low T if extended patches of a perfect (100) surface (of several atomic layers in height) form. Our algorithm permits atomic jumps only on the (110) surface, i.e., a new atomic position can be accepted only if four corner atoms exist on the layer below. A fourfold position of adatom on a perfect (100) slope is considered as an overhang with respect to the (110) section. Such perfect (100) slopes, however, may appear only on the final stages of the simulation, after the faceted structure forms. Therefore, this cannot introduce artificial effects during the development of faceting. If the adsorbates are removed until extended patches of a perfect (100) surface appear, the relaxation to a flat surface at low T occurs slowly. At high T, however, a flat surface is restored rapidly after the adsorbates are removed, as shown in Figs. 12 and 13(b).

VI. DISCUSSION

Of all surface reactions with interesting nonlinear properties catalytic CO oxidation on a Pt(110) surface is clearly the most thoroughly studied system and by far the system with the richest variety of phenomena: rate oscillations, reaction-induced roughening/faceting, different types of chemical wave patterns including standing waves, ''soliton-like'' traveling wave fragments, chemical turbulence, and complex wave patterns associated with reversible roughening/faceting of the surface have all been found on

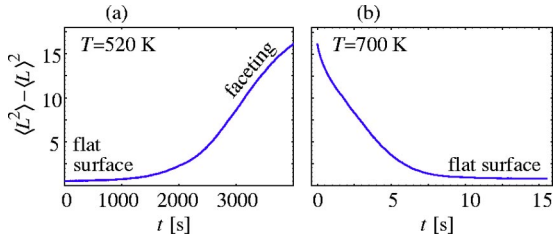

FIG. 13. The variance of atomic layers as a measure of height dispersion of the top Pt atoms. (a) The variance increases due to atomic transport caused by the kinetic instabilities. The faceted state is characterized by a high variance of top atom layers. (b) Simulation of the thermal reordering process for a faceted surface at $T=700$ K, $p_{CO}=0$, $p_{O_2}=0$, $\theta_{CO}=0$, and $\theta_O=0$. A flat surface is restored during the heating.

Pt(110).[41,44,45] Recent studies suggested that in addition to chemisorbed oxygen and CO an additional species, so-called subsurface oxygen might be present under certain conditions and might be responsible for some of the phenomena such as the standing wave patterns.[46] Most of the chemical wave patterns with the exception of those including reversible roughening/faceting have been satisfactorily explained with reaction-diffusion equations.

The present simulation extends the range of modeling the Pt(110) system down to nanoscale dimensions. Nearly all essential experimental observations on reaction-induced roughening/faceting have been reproduced by these simulations with the correct time and length scale.

(i) The different regimes of reaction-induced roughening/faceting in p_{CO}-parameter space.

(ii) The development of facets of the [001] zone during reaction associated with an increase in catalytic activity due to the formation of reactive (100) steps.

(iii) The formation of a periodic hill and valley structure on the faceted surface stabilized by the ongoing reaction.

The severe structural modifications we observe during the reaction are the result of the coupling of a kinetic instability with the mass transport of Pt atoms given in this specific system by the $1\times2\rightleftharpoons1\times1$ surface phase transition. The strong dynamics which are generated in this way may lead to a complete restructuring of the surface creating very open and reactive substrate configurations which decay in the absence of the stabilizing reaction. The catalyst itself thus represents a dissipative structure shaped by the reaction. A critical point is certainly whether the roughening/faceting is coupled with the formation of subsurface oxygen or an oxidelike species.[47] This point needs to be clarified in future experiments because such a connection would provide an additional thermodynamic stabilization of the facets. Experimentally, even an oxide species would be found, it would be rather difficult to decide whether such a species is a byproduct of roughening/faceting or the actual driving force.

Clearly with a simplified model used here not all details seen experimentally can be reproduced. For example, only single atomic (100) steps were seen on the faceted surface in experiment, whereas our simulations allow the generation of multiple height (100) steps. Furthermore, the increase in the oscillation period which accompanies the development of faceting was not found in the simulations. The complex interplay between roughening/faceting and chemical wave patterns which occurs in the channel-like structures observed with LEEM could not be reproduced for principle reasons because we used an ODE system to describe the adsorbate coverages.[45] In future simulations this aspect could be taken into account by transforming the ODE system into a system of partial differential equations. The more general problem which has to be solved for such simulations is that of the proper combination of vastly different time and length scales.

VII. CONCLUSIONS

We have developed a nanoscale model of faceting in the $CO+O_2/Pt(110)$ system taking into account realistic values

of activation barriers for single atomic jumps on Pt(110). The Pt–Pt, Pt–CO, and Pt–O interactions have been extracted from recent experimental data and DFT calculations. Our simulations show that the SPT modeled by the KMC method coupled with an ongoing $CO+O_2$ reaction modeled in the mean-field approximation leads to the development of a regular facet pattern, similar to that detected experimentally. This facet pattern forms a periodic hill and valley structure with a lateral periodicity of ~140–170 Å, which is comparable with the experimentally detected value. The simulations reproduce the region in p_{CO} parameter space where faceting occurs. The development of single (100) microfacets is associated with an increase in catalytic activity, since the (100) microfacets are characterized by a high oxygen sticking coefficient. In our simulations, the faceting process evolves on a realistic time and length scale.

ACKNOWLEDGMENT

This research was supported by the German-Israeli Science Foundation.

APPENDIX: COMPUTATION ALGORITHM

In this appendix, the computation procedure for one MCS is presented. Only atoms occupying free top positions (i.e., not covered by any neighboring atom in the higher layer) are allowed to move. The KMC algorithm shifts the atoms between lattice nodes according to the following rules:

(1) A random free atom is selected on the lattice.

(2) For the chosen free atom, possible jump positions are determined. Any atom can jump only to a free adjacent position in the same layer, in the layer above or below, as shown in Fig. 4(c). Each of 16 possible positions (eight positions in the same layer, four positions in the layer above, and four positions in the layer below) has to be checked. An accepted atomic position should be propped up by four corner atoms of the lower layer. Periodic boundary conditions are applied at the lattice boundaries.

(3) The coordination numbers n of the chosen atom, NN atoms, and sites adjacent to each ith path are determined. The site type is determined in the following way: if the atom has only one of the two $[\underline{1}10]$ NN atoms, it is a (100) step site; if there are two $[110]$ NN atoms, it is a (110) terrace site. The energy of the current position E_0 and the activation barriers for each possible jump ΔE_i^0 are evaluated. Corrections to the surface energy and activation barriers are calculated by Eqs. (14)–(23), where CO and O coverages on different sites are taken from the previous time step. The set of transition probabilities P for all possible jumps is computed according to Eq. (24).

(4) A random number R uniformly distributed between zero and unity is drawn, and a new position is chosen randomly among the available vacant sites with $P_i > R$. If $P_i < R$ for each ith path, no jump is executed and the calculation returns to step 1.

(5) After a new position is selected, the atom is removed from the old position, i.e., the layer tag of the respective site is reduced by two; the layer tag of the new site is increased by two as shown in Fig. 14, and the computation returns to step 1.

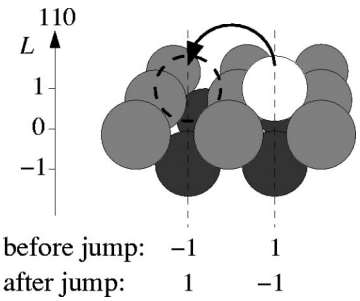

FIG. 14. Change of the atomic layer tag L at two lattice nodes associated with one jump.

This procedure is repeated $2N^2$ times. Following this, time is incremented by Δt. The numerical data are collected: x_{CO}, x_O^{110}, and x_O^{100}, fractions of the surface phases $\theta_{1\times1}$ and $\theta_{1\times2}$. New CO and O coverages θ_{CO}, θ_O^{110}, and θ_O^{100} for the next time step are calculated according to Eqs. (1)–(3) with updated y_{CO}, y_O^{110}, and y_O^{100}. Integration of the ODEs is carried out by means of the Runge-Kutta method.

[1] M. Flytzani-Stephanopoulos and L. D. Schmidt, Prog. Surf. Sci. **9**, 83 (1979).
[2] X. Bao, G. Lehmpfuhl, G. Weinberg, R. Schloegl, and G. Ertl, J. Chem. Soc., Faraday Trans. **88**, 865 (1992).
[3] T. C. Wei and J. Phillips, Adv. Catal. **41**, 359 (1992).
[4] S. Ladas, R. Imbihl, and G. Ertl, Surf. Sci. **197**, 153 (1988).
[5] S. Ladas, R. Imbihl, and G. Ertl, Surf. Sci. **198**, 42 (1988).
[6] M. Sander, R. Imbihl, and G. Ertl, Surf. Sci. **251**, 921 (1991).
[7] M. Sander and R. Imbihl, Surf. Sci. **255**, 61 (1991).
[8] J. Falta, R. Imbihl, M. Sander, and M. Henzler, Phys. Rev. B **45**, 6858 (1992).
[9] R. Imbihl, Mod. Phys. Lett. B **6**, 493 (1992).
[10] R. Imbihl, A. E. Reynolds, and D. Kaletta, Phys. Rev. Lett. **67**, 275 (1991).
[11] T. Gritsch, D. Coulman, R. J. Behm, and G. Ertl, Phys. Rev. Lett. **63**, 1086 (1989).
[12] P. Thostrup, E. Christoffersen, H. T. Lorensen, K. W. Jacobsen, F. Besenbacher, and J. K. Nørskov, Phys. Rev. Lett. **87**, 126102 (2001).
[13] P. Thostrup, E. K. Vestergaard, E. Laegsgaard, and F. Besenbacher, J. Chem. Phys. **118**, 3724 (2003).
[14] M. Sander, R. Imbihl, R. Schuster, J. V. Barth, and G. Ertl, Surf. Sci. **271**, 159 (1992).
[15] Han Wei, Doctoral Thesis, Clausthal, 2003; Han Wei, G. Lilienkamp, and R. Imbihl, Chem. Phys. Lett. **389**, 284 (2004).
[16] P. Hanesch and E. Bertel, Phys. Rev. Lett. **79**, 1523 (1997).
[17] P. Fery, W. Moritz, and D. Wolf, Phys. Rev. B **38**, 7275 (1988).
[18] I. K. Robinson, P. J. Eng, C. Romainczyk, and K. Kern, Surf. Sci. **367**, 105 (1996).
[19] C. Reichert, J. Starke, and M. Eiswirth, J. Chem. Phys. **115**, 4829 (2001).
[20] K. Krischer, M. Eiswirth, and G. Ertl, J. Chem. Phys. **96**, 9161 (1992).
[21] T. R. Linderoth, S. Horch, E. Lægsgaard, I. Stensgaard, and F. Besenbacher, Surf. Sci. **402**, 308 (1997).
[22] T. R. Linderoth, S. Horch, L. Petersen, S. Helveg, E. Lægsgaard, I. Stensgaard, and F. Besenbacher, Phys. Rev. Lett. **82**, 1494 (1999).
[23] T. R. Linderoth, S. Horch, L. Petersen, S. Helveg, M. Schønning, E. Lægsgaard, I. Stensgaard, and F. Besenbacher, Phys. Rev. B **61**, R2448 (1999).
[24] F. Montalenti and R. Ferrando, Phys. Rev. Lett. **82**, 1498 (1999).
[25] P. J. Feibelman, Phys. Rev. B **61**, R2452 (2000).
[26] U. Kürpick, Phys. Rev. B **63**, 045409 (2001).
[27] K.-Dong Shiang and T. T. Tsong, Phys. Phys. B **51**, 5522 (1995).
[28] Q. Ge and D. A. King, J. Chem. Phys. **111**, 9461 (1999).
[29] E. G. Seebauer and C. E. Allen, Prog. Surf. Sci. **49**, 265 (1995).
[30] K. Griffiths, T. E. Jackman, J. A. Davies, and P. R. Norton, Surf. Sci. **138**, 113 (1984).
[31] X.-C. Guo, J. M. Bradley, A. Hopkinson, and D. A. King, Surf. Sci. **310**, 163 (1994).

[32] N. Freyer, M. Kiskinova, G. Pirug, and H. P. Bonzel, Surf. Sci. **166**, 206 (1986).
[33] C. T. Campbell, G. Ertl, H. Kuipers, and J. Segner, Surf. Sci. **107**, 220 (1981).
[34] S. Esch, M. Hohage, T. Michely, and G. Comsa, Phys. Rev. Lett. **72**, 518 (1994).
[35] M. Sander, R. Imbihl, and G. Ertl, J. Chem. Phys. **97**, 5193 (1992).
[36] Q. Ge, P. Hu, D. A. King, M.-H. Lee, J. A. White, and M. C. Payne, J. Chem. Phys. **106**, 1210 (1997).
[37] S. Helveg, H. T. Lorensen, S. Horch, E. Lægsgaard, I. Stensgaard, K. W. Jacobsen, J. K. Nørskov, and F. Besenbacher, Surf. Sci. Lett. **430**, L533 (1999).
[38] E. Janin, H. von Schenck, M. Göthelid, U. O. Karlsson, and M. Svensson, Phys. Rev. B **61**, 13144 (2000).
[39] P. J. Feibelman, S. Esch, and T. Michely, Phys. Rev. Lett. **77**, 2257 (1996).
[40] M. Monine and L. M. Pismen, Phys. Rev. E **69**, 021606 (2004).
[41] R. Imbihl and G. Ertl, Chem. Rev. (Washington, D.C.) **95**, 697 (1995).
[42] M. Monine and L. M. Pismen, Catal. Today **70**, 311 (2001).
[43] M. Monine and L. M. Pismen, Phys. Rev. E **66**, 051601 (2002).
[44] M. Eiswirth and G. Ertl, in *Chemical Waves and Patterns*, edited by R. Kapral and K. Showalter (Kluwer, Dordrecht, 1994).
[45] K. C. Rose, B. Berton, R. Imbihl, W. Engel, and A. M. Bradshaw, Phys. Rev. Lett. **79**, 3427 (1997).
[46] A. v. Oertzen, H. H. Rotermund, A. S. Mikhailov, and G. Ertl, J. Phys. Chem. B **104**, 3155 (2000).
[47] B. L. M. Hendriksen and J. W. Frenken, Phys. Rev. Lett. **89**, 046101 (2002).